e-ISSN 2320 –7876 www.ijfans.org
Vol.11,S Iss.1, 2022
 UGC CARE Listed (Group -I) Journal

Engineered Fe_3 Triangle For The Rapid AndSelective Removal Of Aromatic Cationic Pollutants

Sheetal Sheoran,

Assistant Professor in Chemistry, Mahila Mahavidyalaya Jhojhu Kalan, Charkhi Dadri

ABSTRACT:

Heydays, water pollution is proliferating due to widespread industrialization and in- proper planning of its waste, consisting of aromatic hazards [1]. Most industries dispose of the wastewater in their neighborhood areas of the cities, which is directly in touch with several groundwater sources. The wastewater pollutant (specialties the aromatic ones) can easily enter the underground water which in turn contaminants the surface water and consequently harm the human and environment [2-5].

Keywords: pollution, contaminants, industrialization, surface water, aromatic

INTRODUCTION

The area covered with hard rock water easily creates a shortcut route for water pollutant transport easily into the groundwater. In the last few years, the new problem has emerged in developing countries due to increased water pollutant concentration from large industrial activities and human-made chemical products. Disruption of these natural self-regulatory processes takes place due to the presence of the pollutant in the waterways. Most of the problems are being created due to some of the stable chemicals, which are not easily degradable in the living body and gathered to harm organs. These stable chemicals are aromatic dyes [7], organic compounds [8], heavy metals [6], and the compound containing chlorine [9]. Isolation of this organic pollutant from wastewater can increase the cost of drinking water. To overcome the dangerous side effects on human health is one of the most crucial things scientists need to plan. Natural dyes are becoming the main constituent of water pollution and harmful to the aquatic atmosphere [10]. Mainly, dyes are consumed in the textile industry, but large amounts of dye are used to coloring various materials such as leather, food, plastic, and papers. Due to their complicated aromatic structure and xenobiotic basis, nature dyestuffs are highly stable and very difficult to degrade [11]. Even the minute concentration of such aromatic dyes could be highly remarkable in drinking water [12]. In the wastewater, the dye molecules undergo chemical and biological changes, which further decline the solubility of oxygen and destroy aquatic life also [13]. All of the dyes are very dangerous and stable, so they remain in the aquatic system, degrading water quality and human health [14]. Henceforth, the extraction of this hazardous contaminant from the wastewater is essential, and eliminating them is the need of the hour. There are various water purification methods, such as photodegradation, ultrafiltration, coagulation, ozonation, and

adsorption [15]. Due to its high efficiency, easy handling, and economically better performance, the adsorption process has emerged as a new tool in recent times [16].

Nevertheless, the selective adsorbent selection is quite difficult for practical use of adsorption technology [17]. The adsorbent is explored by various researchers nowadays, including clay material, zeolite, biomass, activated carbon etc. for dye removal [18-20]. However, these adsorbents having low adsorption capacity and difficult to separate. Moreover, these adsorbents lack the specific adsorption of the target dye. The coordination complexes are crystalline materials which consist of metal ions/clusters joined through various non-covalent interactions by organic ligands [21]. The coordination clusters have shown a very vast application in the field of gas adsorption and storage [22], chemical sensing [23], drug delivery [24], adsorption [25], pollutant elimination [26], and catalysis [27]. The MOF materials have been exploited for the adsorption and separation of hazardous contaminants, including dyes, from wastewater. Jhung et al. exploited the two MOFs such as MIL- 101 and MIL-53 for the degradation of methyl orange (MO) from wastewater [28]. After this, a number of researchers have been striving hard in this area using MOF materials to arrest various hazardous dyes present in water. They have employed MOF materials of different metal ions such as aluminum [29], chromium [30,31] iron [32,33] cobalt [34] nickel [35] copper [36] and zirconium [37] for the purpose. It has been established that MOFs can be utilized in dye removing applications with different interactions possible between MOF and dye [38] the oxo-bridged metal. Cluster containing carboxylate as bridging ligand have been of great interest over the years owing to their applications in the field of homogenous catalysis due to their variety of oxidation reactions in the industry [39-41]. The oxo bridge trinuclear iron complexes are also exploited for mimics for the transition metal-containing biological activity [42]. These clusters have essential building blocks for higher nuclear species, which lead to the construction of extended lattice in the solid-state as well as biological materials, e.g., ferritins. Henceforth, these oxo bridged iron clusters tend to form various mixed metal or mixed cluster complexes and then study them for the magnetic interactions between these metal ions present close of definite geometry [43-47]. The MOF-235 was formulated as $\{[Fe_3O(1,4\text{- BDC})_3(DMF)_3][FeCl_4]^-(DMF)_3\}$, which is an orange color hexagonal crystal-synthesized from organic ligand benzenetricarboxylate joined to oxo-bridged trinuclear Fe(III) clusters [48]. The MOF-235 came out to be very stable with many electron-deficient groups in its structure and was employed for the adsorption study. Its various electron deficient groups present in the skeleton form strong hydrophobic interactions and hence serve as a better adsorbent for dye removal. However, the research in the field of stable and discrete coordination complexes serving as better adsorbent is scarcely explored. Due to various non-covalent interactions and structure tunability, the coordination complexes can also be exploited for their dye adsorption property of the desired dye i.e., cationic or anionic [49]. Considering the area of oxo bridged clusters, their adsorption property is untouched by the researchers. In this chapter, we have synthesized a trinuclear Fe(III) complex built by carboxylate groups. The $\{Fe_3\}$ was employed to understand the dye adsorption capacity in details. The
$\{Fe_3\}$ was synthesized in excellent yield using the slow evaporation method. Various spectral studies further thoroughly characterized the cluster, and with the help of a single-crystal X-

ray technique, the exact structure of {Fe_3} was elucidated. The molecular formula of cluster, [Fe_3(μ-O)(2Me-ba)$_6$(H_2O)(CH_3OH)$_2$], which has six benzoate ligand bridged between three Fe(III) centers. The beauty of structure is that one oxygen of the carboxylate ligand forms a bridge between three iron(III) atoms. The {Fe_3} exhibited excellent adsorption property, which selectively adsorbs the cationic dyes in the waste water due to cation-π and π-π interactions between aromatic rings of adsorbent and adsorbates and electrostatic interaction between the two. Further, the adsorption process was screened from different parameters such as pH, temperature, and contact time of the reaction. So, the structural tuning of the metal clusters or cages can lead to the designing of new class of materials based on different metal ions for the adsorption of organic pollutants from wastewater.

Experimental protocols

Materials and method

All the experiments were performed under ambient conditions. 2-methoxy benzoic acid was commercially available and purchased from Sigma Aldrich. Anhydrous ferric chloride was purchased from Merck. All the reagent used in this chapter work were reagent grade and used without any purification.

Instrumentation

FTIR spectrum of solid sample of {Fe_3} was performed on the PerkinElmer Spectrum GX spectrophotometer by making the pellets in KBr in the range of 4000–400 cm^{-1}. The melting point of the {Fe_3} was determined employing an open capillary method.

The carbon, hydrogen, and nitrogen (C, H, N) analysis was performed CDRI, Lucknow, India, in Micro-Analytical Laboratory. The electronic spectra were taken with PerkinElmer λ-45 UV visible spectrophotometer. The cuvettes were used in the spectrophotometer with a path length of 1 cm with 10^{-3} M solution in methanol. The bulk purity was checked using the PXRD pattern on a Miniflexll X-ray diffractometer using Cu-Kα radiation. The thermal study was done on the TGA-50H instrument (temperature range 25-800 °C, heating rate 20 ^{0}C min^{-1}).

X-ray crystal structure determination

Single crystal XRD analysis of {Fe_3} was done at 100 K employing a Bruker SMART APEX CCD diffractometer. The data were monitored using graphite monochromated Mo-Kα radiation with the λ = 0.71073 Å. The data reduction with integration was done with SAINT. The Empirical absorption adjustment was carried out with SADABS and determination of the space group was performed with XPREP. Bond length parameters were fixed by DIFX commands. The structures solution was done employing SHELXL-2016/6 and refinement was accomplished on F^2 (full matrix least squares) with SHELXL-2016/6 [50-53]. Anisotropic displacement parameters were adopted for refining H atoms. **Table 1.1** illustrates the crystal data and refinement parameters for {Fe_3}. The CCDC reference number for {Fe_3} is

1953448.

Protocol for adsorption of organic pollutants

The adsorption of organic pollutant under investigation (dye molecules) on the surface of cluster was evaluated by conducting an adsorption experiment in ambient conditions. The stock solution was prepared for various organic pollutants (10 mg/L) such as methylene blue (MB), congo red (CR), methyl orange (MO) and rhodamine B (Rh-B) in double-distilled water. In this way, we have prepared a 10-ppm solution of dyes in water. The pH of the solution of dyes was normalized using 0.1N NaOH and 0.1N HCl. In an experimental setup, 25 mg of orange color crystals were poured into the 75 mL of aqueous solution of dyes in a round bottom flask. The mixture was then stirred at 25 ^{0}C continuously for further few hours. After that, 3 mL of suspension wastaken out from the round bottom flask at regular intervals and subsequently centrifuged for a few minutes. The solutions were then observed by a UV-Vis spectrophotometer to check the concentration by monitoring the characteristicsabsorption peak. Furthermore, the adsorption capacity q_t (mg/g) can be calculatedusing Eq^{n}(1) [1].

Table 1.1. Selected crystallographic parameter for {Fe$_3$}

Empirical formula	C50H52Fe3O22
Formula weight	1172.49
Crystal color	red
Temperature/K	100(2)
Crystal system	monoclinic
Space group	C2/c
a/Å	12.0171(3)
b/Å	21.5310(7)
c/Å	20.7417(5)
α/°	90
β/°	92.5590(10)
γ/°	90
Volume/Å^3	5361.4(3)
Z	4
ρcalc g/cm3	1.4525
μ/mm^{-1}	0.88
F(000)	2429.7
Crystal size/mm^3	0.38
Radiation	Mo K-ά
Independent reflections	41020
wR$_2$(all)	0.0792
wR$_2$	0.0749

Final R indexes [I>=2σ (I)]	0.0316
Final R indexes [all data]	0.0371
Θmin	2.73
Θmax	25.05
GOF	1.0608

Adsorption capacity (q) = $\frac{(C_0 - C_t)}{m} V$ **(1)**

Scheme. 1.1. Synthetic route for the formation of {Fe_3}.

Results and Discussion

Synthetic approach

The synthetic strategy involves exploring the coordination chemistry of a new iron cluster for its adsorption property. In the synthetic protocols, we aimed to synthesize an iron(III) based cluster by employing the easily available bench chemicals 2- methoxy benzoic acid (2Me-ba), NaOH, and $FeCl_3$. The object of the target molecule was to synthesize it by low cost, chemicals for environment friendly applications. The reaction was carried out in a basic medium using the slow evaporation method to isolate {Fe_3}. Our interest in understanding the adsorption process by MOFs orclusters, we have designed the ecofriendly cluster to explore for its adsorption of dye. Previously, the MOF MIL-235, which is an oxo-bridge Fe_3 entity formulated as {$[Fe_3O(1,4\text{-}BDC)_3(DMF)_3][FeCl_4](DMF)_3$} is an orange color hexagonal crystal- synthesized from organic ligand benzenetricarboxylate joined to oxo-bridge trinuclear Fe(III) clusters [48]. The MOF-235 came out to be very stable and has many electron- deficient groups in its structure and was therefore employed for the adsorption study. Inspired by the fascinating features of MOF-235, in this paper we have designed a low cost {Fe_3} cluster using slow evaporation method which was characterized using various spectroscopic tools. The exact structure of {Fe_3} was elucidated, applying single-crystal X-ray technique that reveals the molecular structure of the cluster to be $[Fe_3(\mu_3\text{-}O)(2Me\text{-}ba)_6(H_2O)(CH_3OH)_2]$. The designed cluster was then exploited for its use in the separation of dyes and thus purification of wastewater. Only a few reports are there in the literature in which metal clusters or cages could be used for the selective adsorption of dyes [54].

Structure of $[Fe_3(\mu_3\text{-}O)(2Me\text{-}ba)_6(H_2O)(CH_3OH)_2]$

The balls-stick and wireframe representation of {Fe_3} is shown in **Fig. 1.1 (a, b)**. The

crystallographic data parameters are shown in **Table 1.1**, and the bond angle bond distances are given in **Table 1.2**. {Fe_3} cluster is a trinuclear Fe(III) complex that is formed through the reaction of 2Me-ba with the $FeCl_3$ salt in the mixed solvent of MeOH/H_2O. The {Fe_3} cluster is having monoclinic system with C2/c space group. The molecular formula of {Fe_3} with the help of SC-XRD data has been deduced to be came as [$Fe_3(\mu_3$-O)(2Me-ba)$_6(H_2O)(CH_3OH)_2$] in which six 2-methoxy benzoic acid ligand bind with three Fe(III) atoms. The oxo-bridged complex also has one water and two methanol moieties coordinated to three Fe(III) atoms. The trinuclear complex has three Fe(III) atoms positioned at the corners of equilateral triangle. The coordination environment around every iron atom is satisfied by oxygen donor sites. All the iron centres are six coordinated with distorted octahedral geometry. The five coordination sites around each iron atom are satisfied by an oxygen donor site of carboxylate ligand and remaining coordination sphere is fulfilled by water or methanol ligand. The three Fe(III) are not bonded directly but bridged with the oxygen atom, which is trapped between the three Fe(III) centres. The non-bonded Fe(III) ions have bond distance ranging between 3.283 to 3.294Å. The oxygen atom is situated at the center of the trinuclear system of three iron centres with bond distance ranging from 1.895 Å to 1.899 Å. The oxygen atom bridges as μ_3 perfectly between three iron atoms with the bond angles varying from 119.86^0 to 120.29^0, which almost resemble to the angles of the equilateral triangle **(Fig. 1.1(c))**.

Table 1.2. Selected bond angles and bond distance parameter

Bond angle (degree)		**Bond distances (Å)**	
O1–Fe1–O1	167.35(9)	Fe1–O1	2.0508(15)
O4–Fe1–O1	90.24(6)	Fe1–O1	2.0508(15)
O4–Fe1–O1	90.24(6)	Fe1–O4	1.9796(15)
O4–Fe1–O1	88.69(6)	Fe1–O4	1.9796(15)
O4–Fe1–O1	88.69(6)	Fe1–O004	1.895(2)
O4–Fe1–O4	170.32(9)	Fe1–O11	2.059(2)
O004–Fe1–O1	96.33(4)	Fe2–O2	1.9997(15)
O004–Fe1–O1	96.33(4)	Fe2–O004	1.8990(10)
O004–Fe1–O4	94.84(5)	Fe2–O5	2.0345(15)
O004–Fe1–O4	94.84(5)	Fe2–O7	1.9849(15)
O11–Fe1–O1	83.67(4)	Fe2–O8	2.0352(15)
O11–Fe1–O1	83.67(4)	Fe2–O10	2.0784(16)
O11–Fe1–O4	85.16(5)		
O11–Fe1–O4	85.16(5)		
O11–Fe1–O004	180.0		
O004–Fe2–O2	96.61(6)		
O5–Fe2–O2	88.97(6)		
O5–Fe2–O004	95.91(6)		
O7–Fe2–O2	168.60(6)		

O7–Fe2–O004	94.79(6)
O7–Fe2–O5	89.75(7)
O8–Fe2–O2	87.76(6)
O8–Fe2–O004	94.54(6)
O8–Fe2–O5	169.34(6)
O8–Fe2–O7	91.45(6)
O10–Fe2–O2	85.73(6)
O10–Fe2–O004	177.42(7)
O10–Fe2–O5	85.21(6)
O10–Fe2–O7	82.88(6)
O10–Fe2–O8	84.44(6)
C1–O1–Fe1	129.11(14)
C1–O2–Fe2	135.27(14)
C9–O4–Fe1	136.65(15)
Fe2–O004–Fe1	119.86(5)
Fe2–O004–Fe1	119.86(5)
Fe2–O004–Fe2	120.29(11)
C9–O5–Fe2	128.45(14)

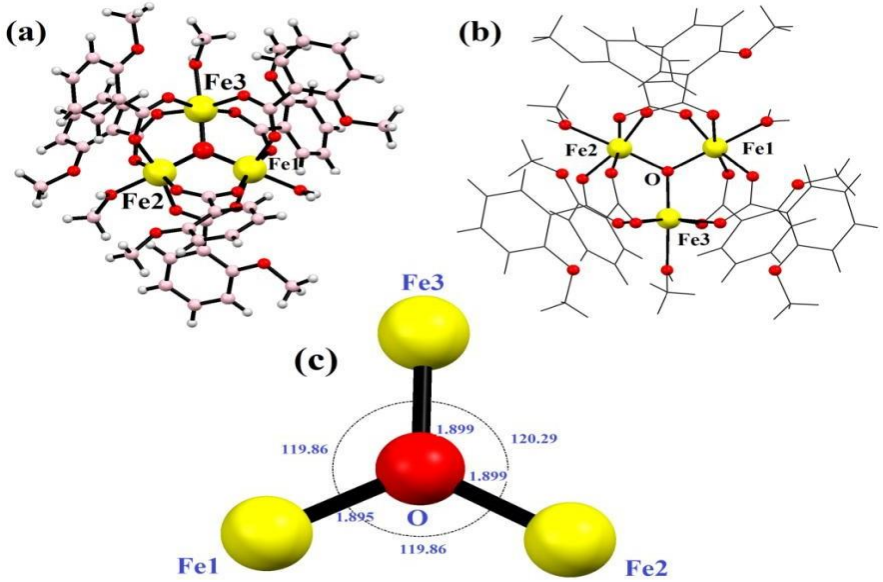

Fig. 1.1. Ball and stick model (a) wireframe structure (b) and the triangle supported by μ_3-O (c) in

{Fe_3}.

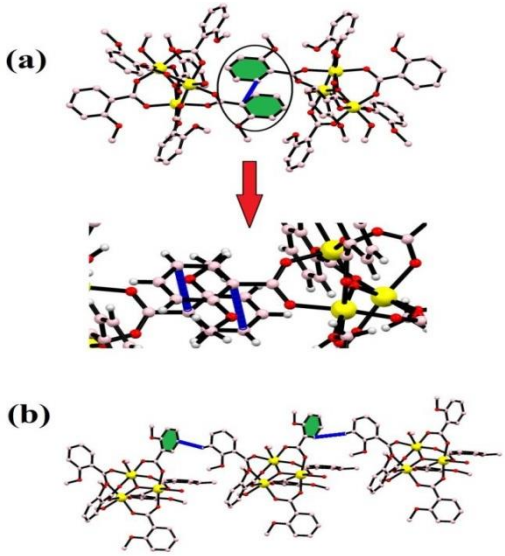

Fig. 1.2. Stability in the {Fe_3} cluster due to π- π (a) and C-H…π (b) interactions.

Every pair of an iron atom is a bridge between two carboxylate ligand and one water or methanol ligand. These bridging carboxylate ligand patterns follow in all the iron atom providing the symmetry in the structure. First of all, Christou et al. reported an iron complex with Fe-Fe bond lengths of 3.253–3.372 Å, similarly bridged by the same two carboxylate ligands [55,56]. The distances between two iron atoms are comparable to our bond distances i.e., 3.283–3.294 Å. In some other reports of other trinuclear $[Fe_3O]^{+7}$ core, the structure does not show the symmetry between the oxo bridge iron(III) complex, and the bond distances range between 1.8–2.0 Å [57–60]. All the six coordination spheres of each iron atom are occupied by the oxygen atom ofcarboxylate ligand and water or methanol solvents. The Fe-O distance between the iron and solvent is in the 2.060 Å and 2.078 Å range. These values are quite similar to the previously reported structures like $[Fe_3O(CH_3COO)_6(H_2O)_3]NO_3{\cdot}4H_2O$ and with some deviation from the $Fe_2(SO_4)_3{\cdot}9H_2O$ and $Fe(NO_3)_3{\cdot}9H_2O$ complexes [59]. The trinuclear iron complex results in an equilateral triangle and T-shaped structure. Moreover, various kinds of non-covalent interactions such as H-bonding, π-π interactions, and C-H…π interactions, provide the formation of supramolecular architecture in {Fe_3} cluster. The formation of H-bonding from the benzoate oxygenof one ligand to the H of other moieties of benzoate ligand led us the formation of supramolecular chain **(Fig. 1.2(a))**. In the same way, π-π interactions and C-H…π are also formed in the {Fe_3} cluster, which provide extra stability and robustness to the complex **(Fig. 1.2(b))**. The π-π interaction was found between the benzoate moieties, which again lead to the formation of a 2-D supramolecular sheet. The C-H…π contacts also exist in the framework, which lead to the formation of a zig-zag chain. All these non-covalent interactions provide extra stability in the complex and the complex is thus quite robust in nature and therefore can further be employed in the high temperature industrial applications. Various overall non-covalent interactions lead to the formation of a 3-

D supramolecular network **(Fig. 1.3)**.

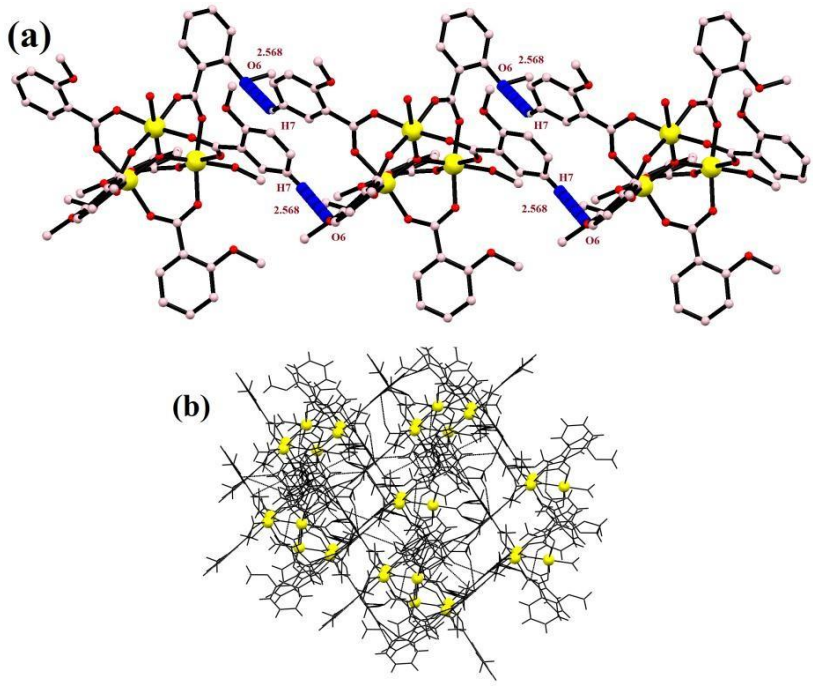

Fig. 1.3. Formation of supramolecular network due various non-covalent interactions in the {Fe_3} cluster.

FTIR, PXRD and TG analysis of {Fe_3} cluster

The FTIR spectroscopy is a technique that provides ample information regarding the binding modes of the ligand with the central metal ion. The FTIR spectrum was obtained in the fingerprint as well as the functional group region. The FTIR spectrum corroborates the single-crystal X-ray information about the {Fe_3} cluster. The FTIR spectrum shows the broad and sharp peaks at 3480 to 3390 cm^{-1} which attributed to the vibration of the water molecule, coordinated to one of the iron atoms in {Fe_3} unit **(Fig. 1.4)**. The band near 1600 cm^{-1} for the C=O band (in free ligand) disappears during the formation of {Fe_3}, which authenticates the complexation of ligand. The spectrum of {Fe_3} cluster further shows a strong band at 1622 and 1364 cm^{-1}, whichis the characteristics of the v_{assym} (COO^-) and v_{symm} (COO^-) vibrations of any carboxylate ligand **(Scheme 1.2)**. These frequencies give ample information about the benzoate binding mode with the Fe(III) atom. The difference between the $v_{assym}(COO^-)$ – $v_{symm}(COO^-)$, which is designed as Δv is the value that providesinformation about the binding mode of carboxylate ligand. In the present {Fe_3} cluster the difference, Δv = 258 cm^{-1} supports the said mode of bonding of benzoate. Theband near at 705 cm^{-1} is due to the C-H bond in the aromatic ring. The band at 1027cm^{-1} is visible in the FTIR spectra, which may be due to the □(C-O) vibration present in the benzoate moieties. The medium intensity bands 546 and 455 cm^{-1} are due to thecoordinate bond of Fe with various benzoate oxygen donors [61]. The new sharp bandat 596 cm^{-1} can be due to the formation of iron and μ_3-O atom [62,

63]. These data are quite informative and further corroborate the single-crystal data. The PXRD pattern ofthe as-synthesized cluster was performed on the crystalline powder sample of {Fe_3}. The simulated pattern was obtained from the single crystal data by MERCURY software. It was seen from the **Fig. 1.5(a)** that the two PXRD patterns are quite identical, which support the bulk integrity of {Fe_3} cluster. The thermal effect on {Fe_3} cluster was analyzed from the TG data. The TG data reveal that the {Fe_3} cluster was relatively stable up to 300 ^{0}C, which may be due to the various non- covalent contacts present in the {Fe_3} cluster. The π-π and C-H…π interactions provide the extra stability to {Fe_3} cluster. The TG analysis of {Fe_3} cluster shows the two-step fragmentation in its structure, where the first step involves the elimination of coordinated water and methanol ligand. In contrast, the second step involves the disintegration of six benzoate ligands. In the first step, the TG reveals the fragmentation of 5.43% weight loss (Calc.: 5.80%) in the range of 25-120 ^{0}C, which may be due to coordinated water and methanol ligands **(Fig. 1.5(b))**. Next, the {Fe_3} cluster was robust and shows a flat curve up to 280 ^{0}C; after that, it shows the removal of six benzoate ligand in the range of 300 ^{0}C to 400 ^{0}C with a weight loss of 64.08% (Calc.: 64.89%). After that, the {Fe_3} cluster does not show any changes up to 600 ^{0}C and the final product left in the {Fe_3} cluster may be oxides or carbon residue whichis the same as that of previous report [64]. Because of the extra stability of {Fe_3} cluster, it can be used in high temperature applications.

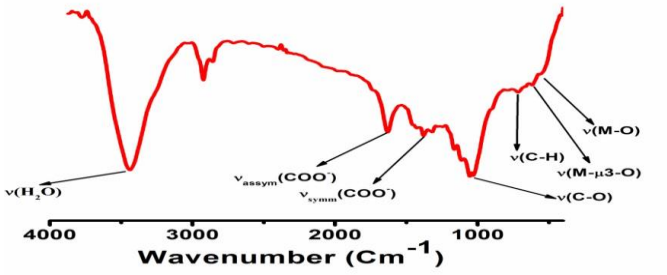

Fig. 1.4. FTIR spectra of {Fe_3} cluster.

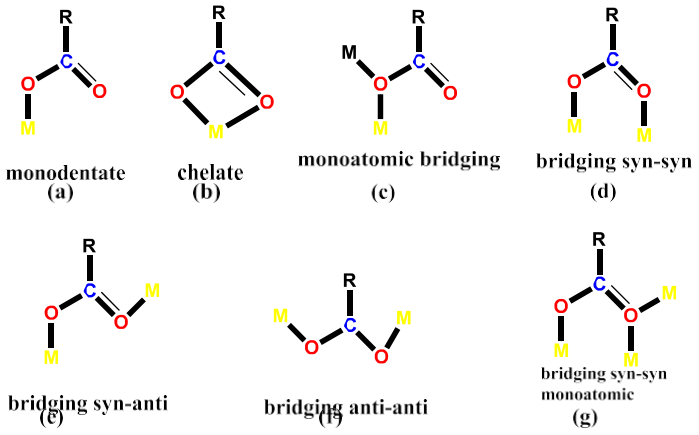

Scheme 1.2. Different coordination modes of carboxylate group present in the benzoate ligand.

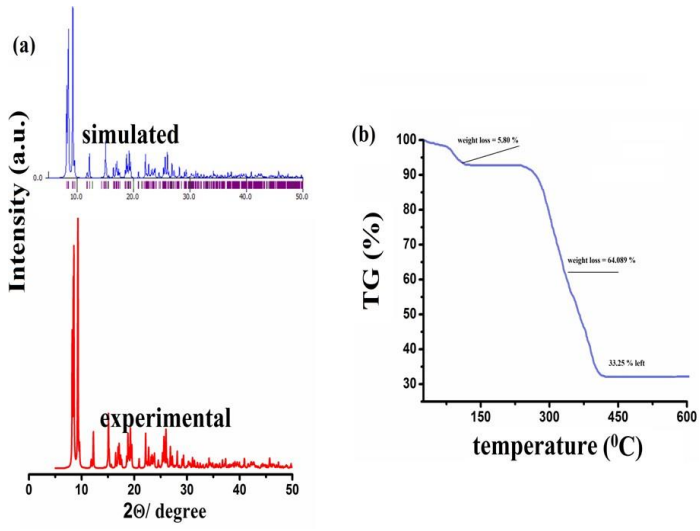

Fig. 1.5. PXRD pattern (a) and TG analysis (b) of {Fe_3} cluster.

Adsorption of organic dyes

Organic pollutants are the main ingredient of sewage from a variety of chemical industries. Almost 700,000 tons of dyes are consumed in the world by the textile manufacture, which is among the top three pollutants. Almost every dye is dangerous and has a high risk of carcinogenic mutations [65]. Due to its environmentally friendly nature and cost-effectiveness, the adsorption process is applied nowadays to remove dye molecules from wastewater [66]. Due to its easy construction method and low-cost constituents, the {Fe_3} cluster was engaged for the adsorption and removal of hazardous dyes from wastewater. In the experiment we have chosen four different dyes i.e., MB, MO, Rh-B, and CR with different charges, and sizes **(Fig. 1.6)** [67].

In a setup, 25 mg of orange color crystals were poured into the 75 mL of aqueous dye solution in a round bottom flask, and the reaction was continuously stirred. Subsequently, 3 mL of aliquot was taken out from the round bottom flask and centrifuged for a few minutes. After that, the different set of the solution was monitored by UV-Vis spectroscopy. The characteristic peak of the dye solution was monitored to understand their concentration. The electronic spectra reveal that the cluster possess a good adsorption capability towards all the cationic dye. The dye adsorption percentage was calculated using the Eq^n (2) [68].

$$\text{Efficiency } (\%) = [(C_0 - C_t)/C_0] \times 100\ \% \quad \textbf{(2)}$$

Where C_0 and C_t are the initial and final concentration of the dyes in mg/L. **Fig. 1.7** illustrates that the cationic dyes show drastic changes in its concentration, while the adsorption of anionic dye does not show appreciable changes in their respective concentrations. The characteristics absorption peaks of MB (664 nm) and Rh-B (553 nm), decreases with the increasing time. The rapid adsorption of cationic dyes occurs at this moment, and in only 60 min, 67.23% of MB and 48.43% of Rh-B dyes were adsorb on the surface of cluster. The adsorption process takes place for 270 min, and after that, the dye molecules resist to adsorb on the surface of {Fe_3} cluster. After 270 min, 92.16% of MB and 79.1% of Rh-B were adsorbed, which is the saturation point for {Fe_3} cluster. We have further extended our adsorption experiment for 12 hrs, but no adsorption occurs after 270 min take place. It can be established very quickly that the rapid adsorption occurs at the starting of the reaction due to cation-π and π-π interactions. In only 150 min, the MB adsorb 83.61% of dye and Rh-B adsorbs 71.8

% of dye molecules, and MB's characteristics color and Rh-B started to decolorize to became transparent. After 270 min, the crystal color of {Fe_3} cluster changes completely from orange to brown in case of MB and pinkish in case of Rh-B adsorption. From the adsorption capacity equation, we have calculated the adsorption of MB and Rh-B by {Fe_3} cluster adsorbent, which is 67.27 and 58.22 mg/g, respectively.

Separation of organic dyes

From an application point of view, the selective adsorption of specific dye is challenging for an environmental chemist. The {Fe_3} cluster efficiently adsorbs the cationic dye, so in an extension of our work, we have further checked whether {Fe_3} cluster can selectively adsorb the cationic dye or not. We have performed an independent experiment in the wastewater, where we have mixed two different dyes for investigations. The {Fe_3} cluster effectively adsorbs the cationic dyes such as MB and Rh-B in the presence of MO and CR as evident from **Fig. 1.8**. On the other hand, we have also performed the adsorption of any single cationic dye even in the presence of two anionic dyes. **Fig. 1.9** demonstrates that the cluster can easily adsorb cationic dye in the presence of any anionic dyes. In this way, we can say that {Fe_3} cluster not only adsorb the cationic dye but also selectively separates the dye from the mixture of anionic and cationic dye solution. This selective adsorption process is somehow typical in MOF or cluster and hence but this becomes first report for a discrete {Fe_3} cluster.

Recyclability of {Fe_3} adsorbent

From its material importance, the reusability of {Fe_3} cluster is a crucial task. After completing the adsorption process, we remove the crystals and perform a separate stirring reaction of the crystal in a small amount of ethanol. The reaction for a few hours until no amount of MB was found on the orange color {Fe_3} cluster. Next, crystals were delicately washed with water and dried in air and in electric oven for 30 min. After that, the {Fe_3} cluster can be reused for further adsorption process. For the second and third cycles, the

adsorption capacity of {Fe_3} cluster decreases due to littlesolubility of {Fe_3} cluster in water, but it can be used for at least three times with better adsorption capacity **(Fig. 1.10(a))** [69].

Effect of pH on the adsorption process

For an adsorption process, the pH of the reaction is an essential parameter from its application point of view. The pH can easily affect the charge on the adsorbent, degree of ionization of dye molecules, and dyes' structure. For this aim in our mind, we have firstly check the PXRD data at different pH ranges from 2 to 12 which reveals that the {Fe_3} is quite stable at different pH. The pH of adsorption reaction should be kept constant throughout the process; for this purpose, firstly, you have to know that optimum pH at which your adsorbent shows the highest adsorption capacity. For this purpose, we have performed adsorption experiment at different pH ranging from 2 to 12 using 0.1N HCl and 0.1N NaOH. All the cationic dyes show a similar pattern at different pH of the reaction. At lower pH, i.e., at pH = 2, the adsorption capacity lowers down as H^+ ion of acid competes with the cationic part of the dye molecules. So, at very low pH, the adsorption capacity is lower and increases with the increasing pH. The adsorption capacity is highest at pH = 7 due to the neutralmedium of the reaction. When we increase the pH from its neutral value, the adsorption capacity decreases due to the negative part of dye that can quickly form a salt with NaOH, and the adsorption capacity decreases significantly. So, it is clear from **Fig. 1.10(b)** that the optimum pH of the reaction is 7, where the highest amount of dye adsorption occurs by {Fe_3} cluster. At pH 2, the adsorption capacity is 22.1 mg/gin case of MB which increases at pH = 5. The adsorption capacity however, in the case of MB at neutral pH is 67.27 mg/g which is higher than different medium.

Moreover, at higher pH again the adsorption capacity of MB decreases and at pH-12 the adsorption capacity is reported to be only 12.01 mg/g [70].

Effect of temperature on the adsorption process

The adsorption process was further assessed at different temperatures ranging from 25 ^{0}C to 50 ^{0}C to understand thermal effect on adsorption. As shown in **Fig. 1.10(c)**, the adsorption of MB at ambient temperature, i.e., at 25 ^{0}C, is highest and as we increase the temperature from 25 ^{0}C to 50 ^{0}C, the adsorption capacity of {Fe_3} cluster decreases significantly. At the 25 ^{0}C, the adsorption capacity is 67.27 mg/L where at
40 ^{0}C that decreases to 43.98 mg/L. Further increment in the temperature, the adsorption capacity decreases significantly, which suggested that the adsorption process follows an exothermal reaction [71].

Effect of contact time on the adsorption process

The contact time is also an essential parameter for assessing organic pollutants' adsorption process from aqueous solutions. As shown in **Fig. 1.10(d)** at the starting of a reaction, the adsorption process takes place very rapidly. In only 30 min, 55.16 mg/gof MB and 19.5 mg/g of Rh-B dye adsorbed by the {Fe_3} cluster. After reaching a saturation point or when the

equilibrium reached, the adsorption process got slow. Itis established here that in case of all the cationic dyes the equilibrium reached in only 90 min of the reaction. This rapid adsorption process may be due to the starting of the reaction; there were various sites available in the {Fe_3} cluster to accommodate the cationic dyes, but after few minutes, when these vacant sites began to occupy, the adsorption process got slow. After 270 min, the {Fe_3} cluster resists adsorbing any further amount, and the adsorption efficiency hence decreases [72].

The PXRD pattern was performed on the adsorbent after completion of first adsorption cycle which suggests that no evidence of breaking of framework of {Fe_3} take place during adsorption process **(Fig. 1.11)**. We have observed the PXRD pattern at different pH which suggest that the cluster is quite stable at different pH **(Fig. 1.12).**

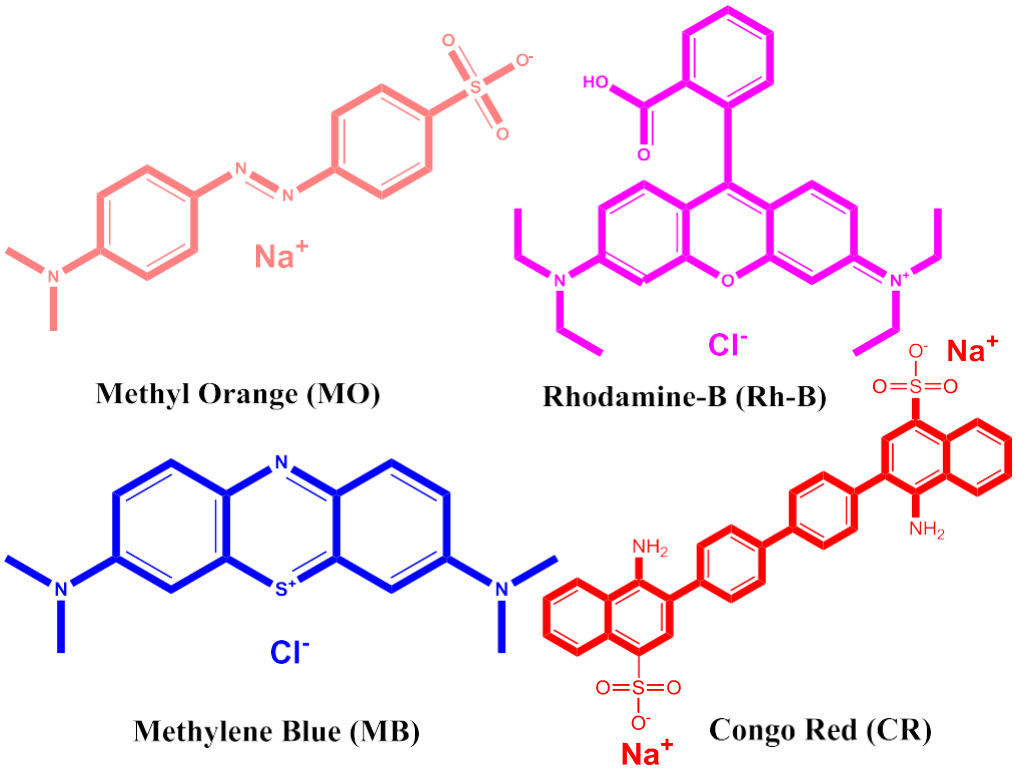

Fig. 1.6. Chemical structures of cationic and anionic dyes used in the experiments.

Adsorption kinetics

As we have witnessed, the {Fe_3} adsorbs the significant amount of cationic dye on its surface, forcing us to perform the reactions' kinetics. To explore the kinetic study of the reaction, the adsorption process was observed with increasing time. Three different kinds of kinetic models were employed to understand the kinetics of the adsorption process: pseudo-first-order, pseudo-second-order, and intraparticle diffusion models [73] and calculated kinetic parameters were given in **Table 1.3**.

Pseudo first order equation

$$\log(q_e - q) = \log q_e - \frac{k_1}{2.303} t \quad \textbf{(3)}$$

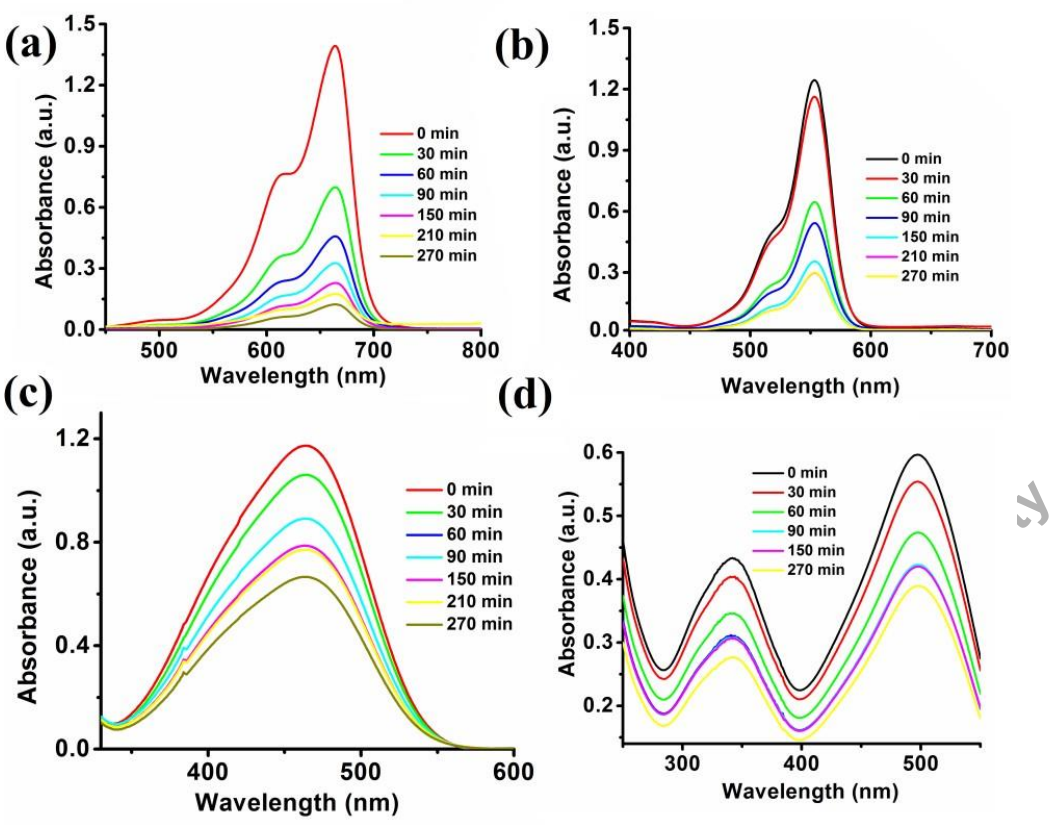

Fig. 1.7. Adsorption of organic dyes such as MB (a), Rh-B (b), MO (c) and CR (d) on UV-Visiblespectrophotometer using {Fe_3} cluster as an adsorbent.

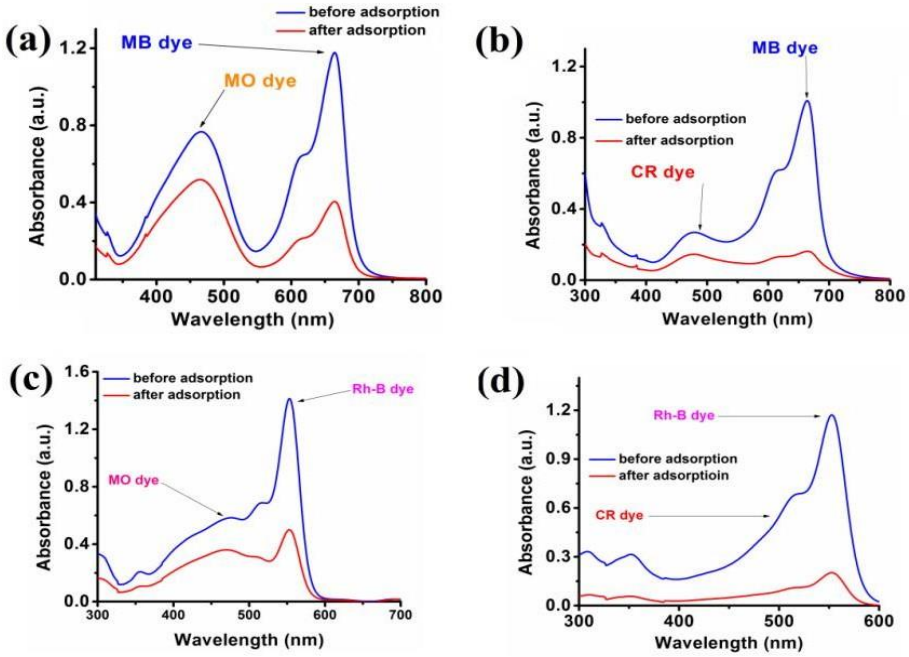

Fig. 4.8. Adsorption of MB (a, b) and Rh-B (c, d) in the presence of MO and CR using {Fe_3} cluster asan adsorbent.

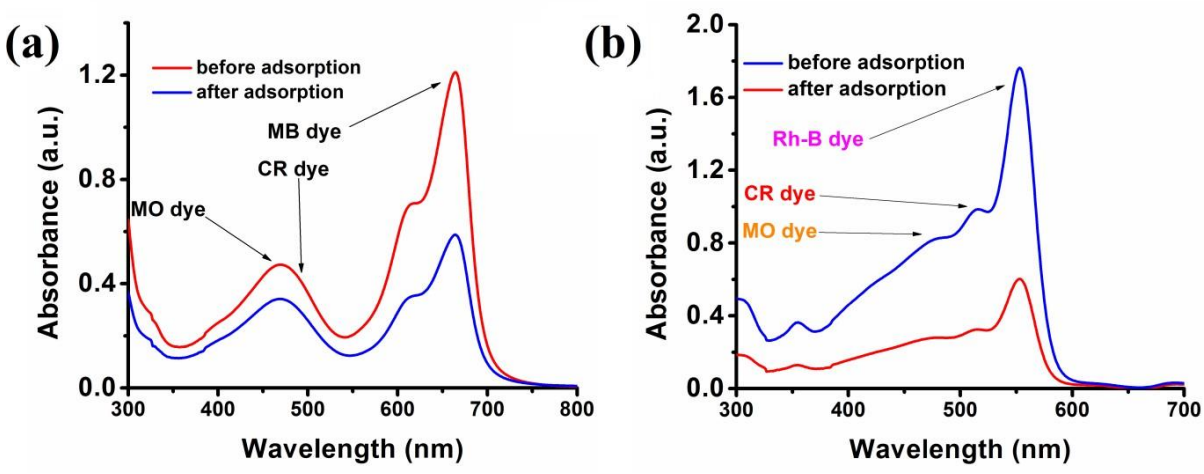

Fig. 1.9. Adsorption of MB (a) and Rh-B (b) in the presence of CR and MO dyes.

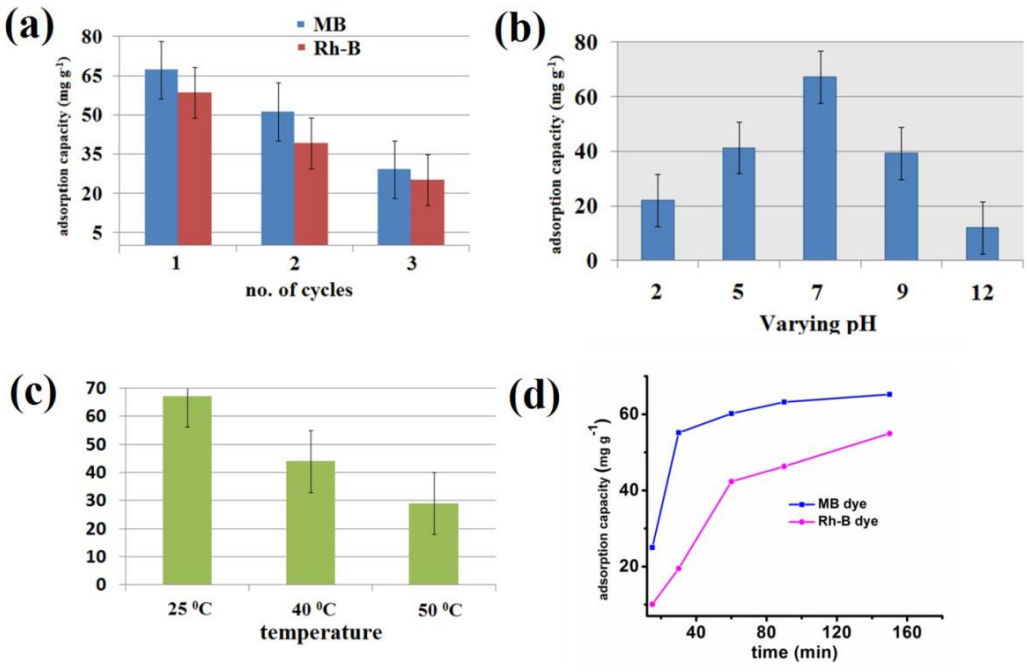

Fig. 1.10. Recyclability of adsorbent (a) effect of pH (b) effect of temperature (c) and effect of contacttime on the adsorption process (d).

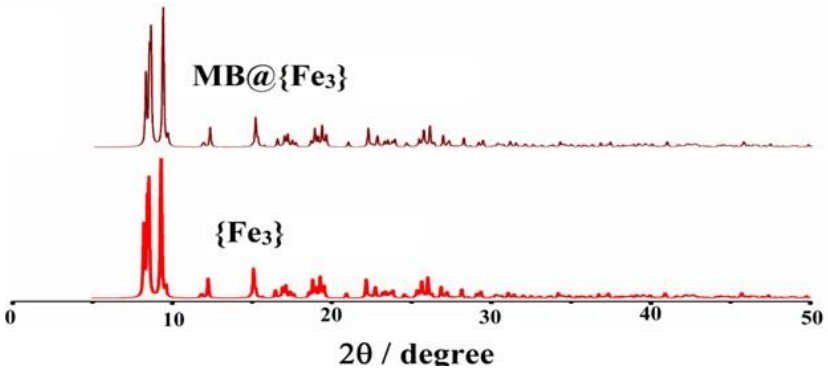

Fig. 1.11. PXRD pattern of adsorbent {Fe_3} cluster before and after adsorption of MB dye.

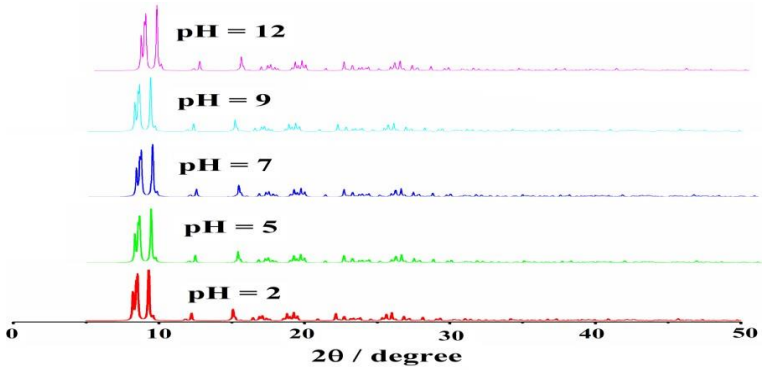

Fig. 1.12. PXRD pattern of adsorbent {Fe_3} at different pH.

Where q_e is the adsorption capacity at equilibrium, q_t is equilibrium capacity at different time t, k_1 is the pseudo-first-order rate constant of the reaction. The rate constant was calculated employing the rate equation, i.e., from the slop between $\log(q_e - q_t)$ and time. The rate constant is quite comparable to the literature reports, butthe values of R^2 are inconsistent from the graph. Moreover, the experimental and calculated adsorption capacity values are quite different from each other, which authenticate this model's inapplicability from the adsorption data **(Fig. 1.13)**.

Pseudo-second-order rate equation

$$\frac{t}{q_t} = \frac{1}{k_2 q_e^2} + \frac{t}{q_t} \quad \textbf{(4)}$$

Again, k_2 is the rate constant of the pseudo-second-order, which is calculated from thegraph between t/q_t and different time intervals. The pseudo-second-order plot shows excellent linearity in its pattern, and the value of the correlation coefficient is very close to zero. Moreover, the values of calculated and experimental adsorption capacities are quite similar. Therefore, this model is suitable for showing the adsorption of organic dyes.

Intra particle diffusion equation

$$q_t = k_3 t^{1/2} \quad \textbf{(5)}$$

Where q_t is the adsorption capacity at a definite time, k_3 is the rate constant for the intraparticle model, and C is the intercept calculated from the graph between q_t and $t_{1/2}$. The inconsistent values of calculated and experimental values of adsorptioncapacities suggest that this model is not suitable for cationic dyes' adsorption kinetics.

Adsorption mechanism

At discrete level, the electrostatic, non-covalent, van der Waals interactions play a keyrole to

bind the dye with either free functionalize groups or available lewis acid/base sites in cluster [54]. It is a well-known fact that the adsorption is a surface phenomenon, and it largely depends upon the structural and functional behavior of the adsorbent, size, and shape of the adsorbate, and surface characteristics of the adsorbent. There are various possible mechanisms reported in the literature for the adsorption process, i.e., acid-base interaction, electrostatic interactions, π–π interactions, hydrogen bonding, and ion exchange mechanism. Form the structure of{Fe_3} cluster; it can be seen that there is possibility of cation-π, π–π, and electrostatic interactions. In the case of {Fe_3} cluster, the presence of the benzoate ring's nucleophilic nature interacts with the cationic part of the dye, which forces the strong electrostatic interaction between the benzoate ring and cationic dyes. Furthermore, the aromatic ring of benzoate ligand provides the strong π–π interactions between the{Fe_3} cluster and the organic dye, which smoothly adsorb the dye on the surface of{Fe_3} clusters. So, we can say that the adsorption process in the case of {Fe_3} cluster is due to various electrostatic interactions and π–π interaction **(Fig. 1.14)**. One more rationale which could be assumed for the rapid adsorption process might be the structural feature of the dye i.e., linearity and the charge of the cationic dye. Thus, we can say that apart from all the interactions, the linear molecules of dyes can be readily adsorbed on the surface of {Fe_3} clusters, which is quite similar to the previous report [74]. Moreover, the oppositely charged (cationic) dyes are interacted towards the nucleophilic center of the aromatic of the rings which also contributes to the efficient adsorption [74]. Furthermore, various Fe-based materials and their adsorption performance towards organic pollutants are documented in **Table 1.4**.

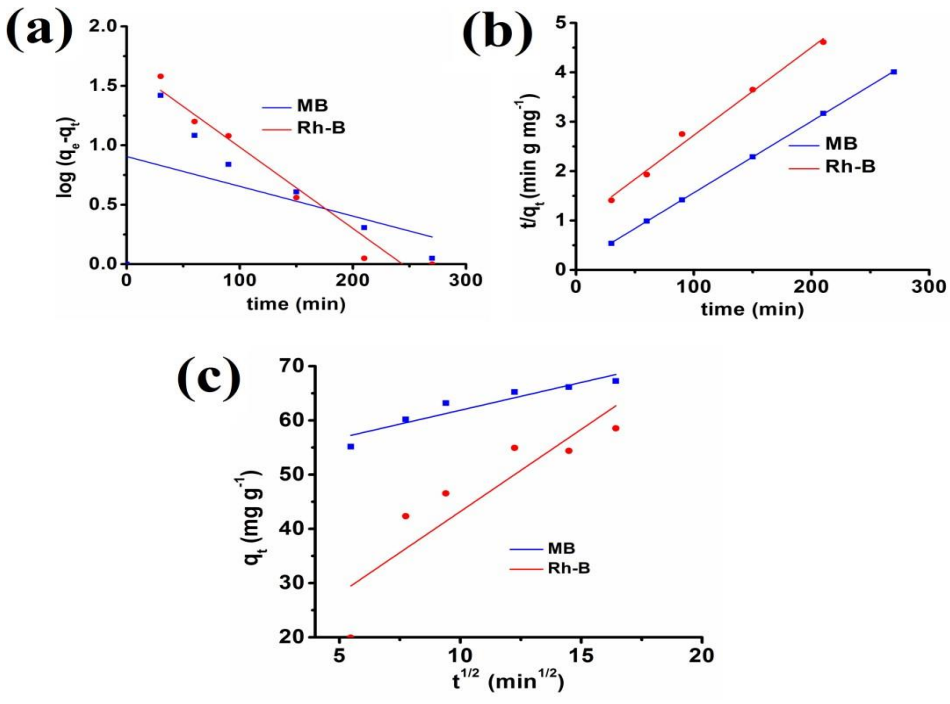

Fig. 1.13. The adsorption of MB and Rh-B onto {Fe_3} cluster using pseudo-first-order (a), pseudo-second-order (b) and intra particle (c) kinetics models.

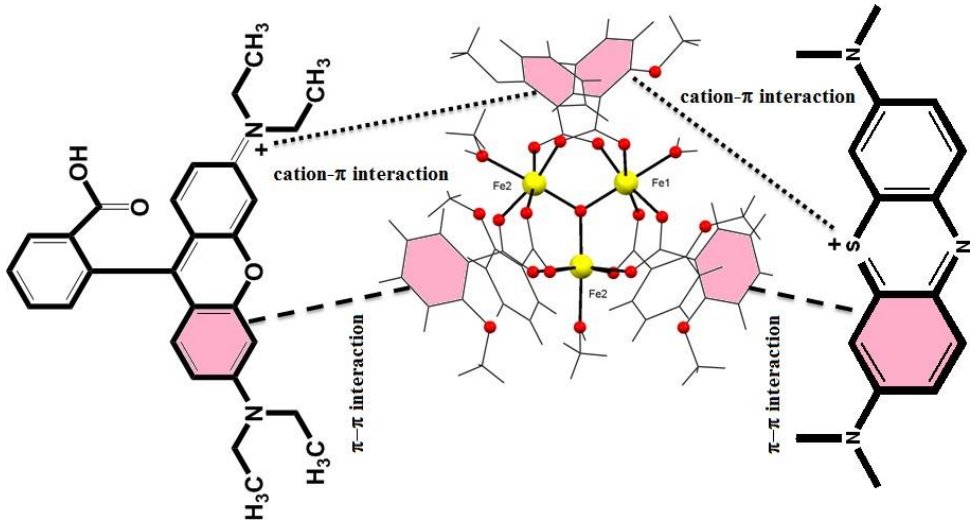

Fig. 1.14. Plausible mechanism for the adsorption of MB and Rh-B using low coast {Fe_3} cluster.

Table 1.3. Parameters for different kinetic models for adsorption studies of MB and Rh-B

Model	Parameters	MB	Rh-B
Pseudo first order	K_1 (min^{-1})	0.0057	0.0156
	q_e (Cal.) (mg/g)	7.94	46.55
	qe (Exp.) (mg/g)	67.27	58.52
R^2		0.94	0.94
Pseudo second order	K_2 (g mg^{-1} min^{-1})	0.00179	0.0005
	q_e (Cal.) (mg/g)	69.44	61.66
	q_e (Exp.) (mg/g)	67.27	58.52
R^2		0.999	0.998
Intraparticle Diffusion	K_3 (mg g^{-1} $min^{-1/2}$)	1.024	3.03
	C	51.64	12.84
R^2		0.8635	0.74

Table 1.4. Iron-based materials with maximum adsorption capacities (q_{max}) towards organic dyes

Materials	Organic Pollutant	Adsorption Capacity/removal efficiency	Ref.No.
Fe-MIL-101	Methylene Blue	124.07 mg g^{-1}	74
MIL-100 (Fe)	Methylene Blue	1045.2 mg g^{-1}	75
NMIL-100 (Fe)	Rhodamine-B	68.69 mg g^{-1}	76
MOF-235	Congo Red and Lemon Yellow	1250 & 250mg g^{-1}	77
Fe-BDC MOF	Methylene Blue	92%	78
MIL-101(Fe)@PDopa@Fe_3O_4	Methyl red	1250 mg g^{-1}	79
{Fe_3} cluster	Methylene Blue, Rhodamine-B	67.27, 58.52 mg g^{-1}	This Work

CONCLUSION

In this paper, we have designed an oxo-bridged low cost {Fe_3} cluster by the slow evaporation method. The {Fe_3} cluster is characterized using spectral techniques, and with the assistance of single-crystal XRD, the exact structure of {Fe_3} cluster was confirmed. The {Fe_3} cluster was then used as an adsorbent for the organic dye such as MB, Rh-B, and CR in the wastewater. The kinetics experiment was also performed to understand the exact mechanism behind the adsorption of organic pollutants. The proposed mechanism is also elaborated, which suggests the cation-π and π-π interaction and other electrostatic interactions are possible for the adsorption process. Thus, the present work is a crucial instance of the structure-activity relationship and the excellent adsorption performance of a low cost {Fe_3} cluster.

REFERENCES

[1] F. Mehrabi, A. Vafaei, M. Ghaedi, A. M. Ghaedi, E. A. Dil, A. Asfaram, *Ultrason. Sonochem*., 2017, **38**, 672.
[2] M. S. Khan, M. Khalid, M. Shahid, *Mater. Adv*., 2020, **1**, 1575.
[3] R. Soury, M. Jabli, T. A. Saleh, W. S. Abdul-Hassan, F. Loiseau, C. Philouze, A. Bujacz, H. Nasri, *J. Mol. Liq*., 2018, **264**, 134.
[4] M. S. Khan, M. Khalid, M. S. Ahmad, M. Shahid, M. Ahmad, *Res. Chem. Intermed*., 2020, **46**, 2985.
[5] N. Tka, M. Jabli, T. A. Saleh, G. A. Salman, *J. Mol. Liq*., 2018, **250**, 423.

[6] V. K. Gupta, A. Nayak Suhas, S. Agarwal, M. Chaudhary, I. Tyagi, *J. Mol.Liq.*, 2014, **190**, 215.
[7] M. Ghaedi, A. M. Ghaedi, E. Negintaji, A. Ansari, A. Vafaei, M. Rajabi, *J.Ind. Eng. Chem*., 2014, **20**, 1793.
[8] J. G. Speight, Environmental Organic Chemistry for Engineers, Butterworth Heinemann, 2017, pp. 203.
[9] K. C. Engvild, *Phytochemistry*, 1986, **25**, 781.
[10] B. Song, T. Wang, H. Sun, Q. Shao, J. Zhao, K. Song, L. Hao, L. Wang, Z.Guo, *Dalton Trans*., 2017, **46**, 15769.
[11] A. Ayar, O. Gezici, M. Kuç ¨ ukosmanoglu, *J. Hazard. Mater*., 2007, **146**,186.
[12] K. Elass, A. Laachach, A. Alaoui, M. Azzi, *Appl. Clay Sci*., 2011, 54, 90.
[13] S. Wang, X. Xu, Y. Bai, Y. Ma, J. Zhang, F. Meng, J. Zhao, C. Tang, Sci. *Adv. Mater*., 2016, **8**, 1020.
[14] T. Wang, P. Zhao, N. Lu, H. Chen, C. Zhang, X. Hou, *Chem. Eng. J*., 2016, **295**, 403.
[15] S. Cinar, U. H. Kaynar, T. Aydemir, S. C. Kaynar, M. Ayvacikli, *Int. J. Biol. Macromol*., 2017, **96**, 459.
[16] (a) L. Zhang, M. Qin, W. Yu, Q. Zhang, H. Xie, Z. Sun, Q. Shao, X. Guo, L.Hao, Y. Zheng, Z. Guo, *J. Electrochem. Soc*., 2017, **164**, H1086; (b) V. Gomez, M. S. Larrechi, M. P. Callao, *Chemosphere*, 2007, **69**, 1151.
[17] E. Yilmaz, E. Sert, F. S. Atalay, *J. Taiwan Inst. Chem. Eng*., 2016, **65**, 323; S.Wang, Z. H. Zhu, J. Hazard. Mater., 2006, **136**, 946.
[18] K. Gong, Q. Hu, L. Yao, M. Li, D. Sun, Q. Shao, B. Qiu, Z. Guo, *ACS Sustainable Chem. Eng*., 2018, **6**, 7283.
[19] S. S. Tahir, N. Rauf, *Chemosphere*, 2006, **63**, 1842.
[20] J. Huang, Y. Cao, Q. Shao, X. Peng, Z. Guo, *Ind. Eng. Chem. Res*., 2017, **56**,10689.
[21] L. Zeng, L. Xiao, Y. Long, X. Shi, *J. Colloid Interface Sci*., 2018, **516**, 274.
[22] S. Xiong, Y. Gong, S. Hu, S. Wu, W. Li, Y. He, *J. Mater. Chem. A*, 2018, **6**, 4752.
[23] M. Ashafaq, M. Khalid, M. Raizada, M. S. Ahmad, M. S. Khan, M. Shahid, M. Ahmad, *J. Inorg. Organomet. Polym. Mater*., 2020, **30**, 4496.
[24] M. S. Ahmad, M. Khalid, M. S. Khan, M. Shahid, M. Ahmad, M. Rao, A. Ansari, M. Ashafaq, *New J. Chem*., 2020, **44**, 7998.
[25] J. Xu, W. Xing, H. Wang, W. Xu, Q. Ding, L. Zhao, *Analyst*, 2016, **141**, 2307–2319; W. Li, X. Wu, S. Li, W. Tang, Y. Chen, *Appl. Surf. Sci*., 2018,**436**, 252–262.
[26] W. Ren, J. Gao, C. Lei, Y. Cai, Q. Ni, J. Yao, *Chem. Eng. J*., 2018, **349**, 766–774.
[27] M. S. Ahmad, M. Khalid, M. S. Khan, M. Shahid, M. Ahmad, *J. Struct. Chem*., 2020, **61**, 533.
[28] E. Haque, J. E. Lee, I. T. Jang, Y. K. Hwang, J.-S. Chang, J. Jegal, S. H. Jhung, *J. Hazard. Mater*., 2010, **181**, 535.
[29] T. Shen, J. Luo, S. Zhang, X. Luo, *J. Environ. Chem. Eng*., 2015, **3**, 1372.

[30] X. Luo, X. Fu, Y. Du, J. Guo, B. Li, *Microporous Mesoporous Mater*., 2017,
237, 268.
[31] T. Wang, P. Zhao, N. Lu, H. Chen, C. Zhang, X. Hou, *Chem. Eng. J*., 2016, **295**, 403.
[32] S. Luo, J. Wang, *Environ. Sci. Pollut. Res. Int*., 2018, **25**, 5521.
[33] X. Li, W. Guo, Z. Liu, R. Wang, H. Liu, *Appl. Surf. Sci*., 2016, **369**, 130.
[34] R. Rajak, M. Saraf, A. Mohammad, S. Mobin, *J. Mater. Chem. A*, 2017, **5**, 17998.
[35] L. Jin, X. Zhao, X. Qian, M. Dong, *J. Colloid Interface Sci*., 2018, **509**, 245.
[36] M. S. Khan, M. Khalid, M. S. Ahmad, M. Shahid, M. Ahmad, *J. Struct. Chem*., 2019, **60**, 1833.
[37] C. Cabello, M. Pico, F. Maya, M. del Rio, G. Palomino, *Chem. Eng. J*., 2018,
346, 85.
[38] J. Zhang, F. Li, Q. Sun, *Appl. Surf. Sci*., 2018, **440**, 1219.
[39] J. S. Seo, D. Whang, H. Lee, S. I. Jun, J. Oh, Y. J. Jeon, K. Kim, *Nature*, 2000, **404**, 982.
[40] C. E. Summer Jr, G. R. Steinmetz, *J. Am. Chem. Soc*., 1985, **107**, 6124.
[41] S. Ito, K. Inone, M. Mastumoto, *J. Am. Chem. Soc*., 1982, 1**04**, 6450.
[42] S. J. Lippard, *Angew. Chem*., 1988, **100**, 353.
[43] M. C. Ghosh, S. Mandal, S. K. Chandra, S. E. Gould, *Inorg. Chem*., 1995, **34**,509.
[44] C. Stadler, J. Daub, J. K¨ ohler, R. W. Saalfrank, V. Coropceanu, V. Schunemann, C. Ober, A. X. Trautwein, ¨ S. F. Parker, M. Poyraz, T. Inomata, R. D. Cannon, *J. Chem. Soc., Dalton Trans*., 2001, 3373.
[45] Y. T. Lui, C. W. Yan, H. S. Guan, *Polyhedron*, 2003, **22**, 3223.
[46] M. Eshel, A. Bino, *Inorg. Chim. Acta*, 2002, **329**, 45.
[47] A. Harton, K. Terrell, J. C. Huffman, C. MacDonald, A. Beatty, S. Li, C. J. O'Connor, J. B. Vincent, *Inorg. Chem*., 1997, **36**, 4875.
[48] M. Anbia, V. Hoseini, S. Sheykhi, *J. Ind. Eng. Chem*., 2012, **18**, 1149.
[49] H. Duo, H. Tang, J. Ma, X. Lu, L. Wang, X. Liang, *New J. Chem*., 2019, **43**,15351.
[50] J. A. Ibers and W. C. Hamilton, International Tables for X-ray Crystallography, Kynoch Press, Birmingham, England, 1974, vol. IV. 26;SMART & SAINT Software Reference manuals, Version 6.45, Bruker Analytical X-ray Systems, Inc., Madison, WI, 2003.
[51] G. M. Sheldrick, SADABS, software for empirical absorption correction, Ver.2.05, University of G¨ ottingen, G¨ ottingen, Germany, 2002.
[52] XPREP, version 5.1, Siemens Industrial Automation Inc., Madison, WI, 1995.
[53] L. J. Bourhis, O. V. Dolomanov, R. J. Gildea, J. A. K. Howard and H.Puschmann, *Acta Crystallogr., Sect. A: Found. Adv*., 2015, **71**, 59.
[54] K. Iman, M. Shahid, M. Ahmad, *Dalton Trans*., 2020, **49**, 3423.
[55] C. C. Vilalta, E. Rumberger, E. K. Brechin, W. Wernsdorfer, K. Folting, E. R.

Davidson, D. N. Hendrikson, G. Christou, *J. Chem. Soc., Dalton Trans*., 2002,4005.
[56] E. J. Seddon, J. C. Huffman, G. Christou, *J. Chem. Soc., Dalton Trans*., 2000,4446.
[57] X. M. Ren, H. Okudera, R. K. Kremer, *Acta Crystallogr., Sect. E: Struct. Rep. Online*, 2004, **60**, m14.
[58] J. Overgaard, F. K. Larsen, B. Schitt, B. B. Iversen, *J. Am. Chem. Soc*., 2003, **125**, 11088.
[59] K. I. Turte, S. G. Shova, F. A. Spatar, M. D. Mazus, T. I. Malinovskii, *J.Struct. Chem*., 1994, **35**, 248.
[60] A. K. Boudalis, Y. Sanakis, C. P. Raptopoulou, A. Terzis, J.-P. Tuchagues, S. P. Perlepes, *Polyhedron*, 2005, **24**, 1540.
[61] M. S. Khan, M. U. Hayat, M. Khanam, H. Saeed, M. Owais, M. Khalid, M.Shahid, M. Ahmad, *J. Biomol. Struct. Dyn*., 2020, **39**, 4037.
[62] E. Bill, C. Krebs, M. Winter, M. Gerdan, A. Trautwein, U. Fl¨ orke, H.-J.Haupt, P. Chaudhuri, *Chem. - Eur. J*., 1997, **3**, 193.
[63] P. Chaudhuri, M. Winter, P. Fleischhauer, W. Haase, U. Fl¨ orke and H.-J.Haupt, *Inorg. Chim. Acta*, 1993, **212**, 241.
[64] M. S. Khan, M. Khalid, M. S. Ahmad, M. Ahmad, M. Ashafaq, R. Uddin, R.Arif, M. Shahid, *J. Mol. Struct*., 2019, **1175**, 889.
[65] X. Ren, G. Zeng, L. Tang, J. Wang, J. Wan, Y. Liu, J. Yu, H. Yi, S. Ye, R.Deng, *Sci. Total Environ*., 2018, **1154**, 610.
[66] L. Qin, G. Zeng, C. Lai, D. Huang, P. Xu, C. Zhang, M. Cheng, X. Liu, S. Liu, B. Li, H. Yi, *Coord. Chem. Rev*., 2018, **359**, 1.
[67] X. Zhang, Y. Gao, H. Liu, Z. Liu, *CrystEngComm*, 2015, **17**, 6037.
[68] A. Mariyam, M. Shahid, I. Mantasha, M. S. Khan, M. S. Ahmad, J. *Inorg. Organomet. Polym. Mater*., 2019, **30**, 1935.
[69] S. Kamal, M. Khalid, M. S. Khan, M. Shahid, M. Ashafaq, I. Mantasha, M. S. Ahmad, M. Ahmad, M. Faizan, S. Ahmad, *Inorg. Chim. Acta*, 2020, **512**, 119872.
[70] M. S. Khan, M. Khalid, M. S. Ahmad, M. Shahid, M. Ahmad, *Dalton Trans*.,2019, **48**, 12918.
[71] I. Mantasha, H. A. M. Saleh, K. M. A. Qasem, M. Shahid, M. Mehtab, M.Ahmad, *Inorg. Chim. Acta*, 2020, **511**, 119787.
[72] K. Iman, M. Shahid, M. S. Khan, M. Ahmad, F. Sama, *CrystEngComm*, 2019, **21**, 5299.
[73] M. N. Ahamad, M. S. Khan, M. Shahid, M. Ahmad, *Dalton Trans*., 2020, **49**,14690.
[74] S. M. Hassan, A. A. Ibrahim, D. A. Mohamed, *Int. J. Mod. Chem*., 2017, **9**, 111.
[75] M. Tong, D. Liu, Q. Yang, S. Devautour-Vinot, G. Maurin, C. Zhong, *J. Mater. Chem. A*, 2013, **1**, 8534.
[76] S. Duan, J. Li, X. Liu, Y. Wang, S. Zeng, D. Shao, T. Hayat, *ACS SustainableChem. Eng*., 2016, **4**, 3368.
[77] H. Duo, H. Tang, J. Ma, X. Lu, L. Wang, X. Liang, *New J. Chem*., 2019, **43**,

15351.
[78] C. Arora, S. Soni, S. Sahu, J. Mittal, P. Kumar, P. K. Bajpai, *J. Mol. Liq.*, 2019, **284**, 343.
[79] A. Hamedi, M. B. Zarandi, M. R. Nateghi, *J. Environ. Chem. Eng*., 2019, **7**, 102882.